

This discussion paper is/has been under review for the journal Atmospheric Chemistry and Physics (ACP). Please refer to the corresponding final paper in ACP if available.

Simplifying the calculation of light scattering properties for black carbon fractal aggregates

A. J. A. Smith and R. G. Grainger

Atmospheric, Oceanic and Planetary Physics, Clarendon Laboratory, Oxford, OX1 3PU, UK

Received: 20 December 2013 – Accepted: 1 February 2014 – Published: 7 February 2014

Correspondence to: A. J. A. Smith (smith@atm.ox.ac.uk)

Published by Copernicus Publications on behalf of the European Geosciences Union.

Black carbon fractal aggregates

A. J. A. Smith and
R. G. Grainger

[Title Page](#)

[Abstract](#)

[Introduction](#)

[Conclusions](#)

[References](#)

[Tables](#)

[Figures](#)

[|◀](#)

[▶|](#)

[◀](#)

[▶](#)

[Back](#)

[Close](#)

[Full Screen / Esc](#)

[Printer-friendly Version](#)

[Interactive Discussion](#)



Abstract

Black carbon fractal aggregates have complicated shapes that make the calculation of their optical properties particularly computationally expensive. Here, a method is presented to estimate fractal aggregate light scattering properties by optimising simplified models to full light scattering calculations. It is found that there are no possible spherical models (at any size or refractive index) that well represent the light scattering in the visible, or near-thermal infrared. As such, parameterisations of the light scattering as a function of the number of aggregate particles is presented as the most pragmatic choice for modelling distributions of black carbon when the large computational overheads of rigorous scattering calculations cannot be justified. This parameterisation can be analytically integrated to provide light scattering properties for log-normal distributions of black carbon fractal aggregates and return extinction cross-sections with 0.1 % accuracy for typical black carbon size distributions. Scattering cross-sections and the asymmetry parameter can be obtained to within 3 %.

15 1 Introduction

Particulate products of incomplete combustion, such as black carbon (BC), have been the subject of recent intense discussion (e.g. Jacobson, 2002, 2003; Bond, 2007; Bond et al., 2013). Emissions rates are high (Bond et al., 2004), and have tripled in the last 140 yr (Ito and Penner, 2005) although specific regions have not followed this trend.

20 The developed world has reduced emissions while Asian countries have come to dominate carbon aerosol emission (Streets et al., 2003). Since BC has a high imaginary part of refractive index, it is one of the few aerosols that has a positive direct effect on radiative forcing (Jacobson, 2001; Bond, 2007; Bahadur et al., 2011).

Studies have shown that when BC is deposited on snow, the lowering of surface 25 albedo leads to faster run-off and to an additional warming effect (e.g. Flanner et al., 2009; Doherty et al., 2010), although other absorbing aerosols also play a role (Bond

Black carbon fractal aggregates**A. J. A. Smith and
R. G. Grainger**[Title Page](#)[Abstract](#)[Introduction](#)[Conclusions](#)[References](#)[Tables](#)[Figures](#)[|◀](#)[▶|](#)[Back](#)[Close](#)[Full Screen / Esc](#)[Printer-friendly Version](#)[Interactive Discussion](#)

et al., 2013). Aside from the positive radiative forcing due to BC, there are considerable negative health effects from fine particulate matter (Dockery et al., 1993; Jansen et al., 2005), and in urban environments, issues of poor visibility (Larson et al., 1989).

Black carbon fractal aggregates (BCFA) are clusters of BC spherules forming aerosols with a non-spherical shape. Accurate quantification of their optical properties is important both for their measurement, and for predicting their radiative effect. Current estimates of the climate forcing caused by BC emissions are positive with a typical value of 1.1 W m^{-2} (Bond et al., 2013).

The object of this work is to see whether there are spheres (of some radius, r and complex refractive index, m) whose optical properties are close enough to a BCFA's light scattering properties (as calculated using T-Matrix code) to acceptably represent these particles. If some mapping of r and m to properties of the BCFA can be found, there may be additional physical insight into the fractal light scattering, additional to the advantage of a much simpler scattering calculation.

After a brief description of black carbon, we show that this is not possible within the bounds of reasonably sized spheres with a wide range of refractive indices and go on to present a parameterisation of BCFA light scattering properties.

1.1 A physical description of aerosol formation and ageing

Formation of sub-micron aggregate aerosols from burning is a rapid process involving several stages, some of which are irreversible. Initially, due to very high temperatures, some of the burning fuel vapourises (if it is not already gaseous). If the fuel is something such as coal, the main products could be inorganics and elemental carbon formed from the vapoured coal ash (Helble et al., 1988; Turns, 2000). In the case of biomass, this could be organics such as benzene and poly-aromatic hydrocarbons (PAH) (Reid et al., 2005).

Further away from the hottest part of the flame, nucleation of these molecules leads to the formation of very small particles with diameters of 1–2 nm (Calcote, 1981). These quickly grow by coagulation and surface condensation to sizes of 10–30 nm. Coagula-

Black carbon fractal aggregates

A. J. A. Smith and
R. G. Grainger

tion is encouraged initially due to a high proportion of hydrocarbon radicals which falls off as the particles age (Homann, 1967; Calcote, 1981). High resolution TEM images of individual carbonaceous spherules shows them to be haphazardly ordered micro-structures of graphene-like layers (Buseck et al., 1987; Pósfai et al., 1999; Li et al., 2003) with a very narrow range of diameters for a specific flame (Homann, 1967).

After the initial nucleation and coagulation, primary particles can aggregate leading to the fractal soot aerosol often seen (e.g. Helble et al., 1988; Sorensen, 2001; Li et al., 2003; Zhang et al., 2008). As the particles pass through the edge of the flame, some will be oxidised, although not completely (Turns, 2000). Those that make it through the flame without burning are the soot emissions. Flames that burn more intensely have poorer transport of oxygen into the area where the particles are being created, and as a result will emit more particulate matter (Reid et al., 2005).

The aggregates created during burning last a very short amount of time, of the order of hours (Martins et al., 1998b), before being irreversibly deformed as the chain-like structures fold up into more spherical clusters (Martins et al., 1998a; Abel et al., 2003).
15 Although the soot spherules are hydrophobic, their irregular shapes provide active sites where water can be deposited (Zhang et al., 2008). This change is thought to be due to atmospheric processing of the particles by nucleating water, and the coating of the carbon by nucleating additional products of the burning, e.g. sulphate and OC. This also
20 means that the BC cores become coated in shells of other material which are generally hydrophilic (Popovicheva et al., 2008). This coating enhances the light absorption of the BC core (Fuller et al., 1999; Jacobson, 2001; Bond et al., 2006).

1.2 Fractal dimension

Fractal aggregate particles are to some extent scale invariant, although do not have the true scale invariance of a mathematical fractal, which would have infinite extent.

Title Page

Abstract

Introduction

Conclusions

References

Tables

Figures

1

1

Back

[Close](#)

Full Screen / Esc

[Printer-friendly Version](#)

Interactive Discussion



Particles are defined by the equation

$$n_s = k_f \left(\frac{R_g}{a} \right)^{D_f}, \quad (1)$$

where n_s is the number of spherules in the aggregate, a is the radius of an individual spherule in the fractal, D_f is the fractal dimension, k_f is the fractal prefactor, and R_g is the radius of gyration which gives the root-mean-square distance of spherules from the cluster's centre of mass (Sorensen, 2001).

The fractal dimension gives a measure of how “compact” an aggregate is, with lines of particles when $D_f \approx 1$, “flat” surfaces when $D_f \approx 2$, and lumpy spherical shapes as $D_f \rightarrow 3$ (although due to the individual spherules having non-negligible size, it is not possible to form shapes with no free space between constituent parts). This dependence of shape on D_f is shown in Fig. 1.

For particles formed by diffusion limited cluster aggregation (such as soot from flames), fractal dimensions of $D_f \approx 1.75 \rightarrow 1.8$ are expected (Sorensen, 2001).

1.3 Light scattering methods

The scattering of light by a spherical particle can be solved analytically using Mie’s solution to Maxwell’s equations (Mie, 1908; Bohren and Huffman, 1983). Additionally, the derivatives of all light scattering properties are also analytic (Grainger et al., 2004).

The scattering of light by fractal clusters can be calculated using the Multiple Spheres T-Matrix Fortran-90 code (MSTM) (Mackowski, 2012) which is based on theory found in Mackowski and Mishchenko (1996). This method combines the spherical wave expansions for each spherule (at that spherules origin) in the aggregate, and orientationally averages. For this work, the results from this method are considered “correct”.

[Title Page](#)

[Abstract](#)

[Introduction](#)

[Conclusions](#)

[References](#)

[Tables](#)

[Figures](#)

◀

▶

[Back](#)

[Close](#)

[Full Screen / Esc](#)

[Printer-friendly Version](#)

[Interactive Discussion](#)



2 Method

Light scattering properties of BCFAs were calculated over a range of wavelengths, λ , from 400 nm to 15 μm using the MSTM code. The fractal aggregates were generated using a cluster–cluster algorithm (Thouy and Jullien, 1994) with a spherule radius of 5 25 nm and fixed fractal prefactor of $k_f = 1.18$ which is very close to value used by Liu and Mishchenko (2005); Zhao and Ma (2009); Li et al. (2010). For $400 \text{ nm} \leq \lambda \leq 1 \mu\text{m}$, a step size of $\Delta\lambda = 150 \text{ nm}$ and a fixed refractive index of $m_{\text{BC}} = 1.95 + 0.79i$ was selected, following Bond and Bergstrom (2006). Above this, the step size was widened to $\Delta\lambda = 1 \mu\text{m}$ and a parameterised refractive index fit by Chang and Charalampopoulos 10 (1990) was used. To alter the shape and size, the number of spherules was varied in steps of 20 with $20 \leq n_s \leq 980$ and fractal dimension in steps of 0.1 with $1.6 \leq D_f \leq 2.2$. The calculated optical properties were the extinction and scattering crosssections, σ_{ext} , 15 σ_{sca} , and the asymmetry parameter g which gives a measure of the angular distribution of scattered light (Bohren and Huffman, 1983) and is used in several global circulation models to represent aerosol optical properties (e.g. Stier et al., 2007).

Next, best fits of spherical radius and complex refractive index ($m = n + ik$) of spheres were fitted to the individual BCFAs. Optimal estimation (Rodgers, 2000) and least-squares fitting were tried. The differential optical properties required for the inversion, e.g. $\frac{\partial\sigma_{\text{ext}}}{\partial r}$, $\frac{\partial g}{\partial n}$, were obtained using IDL code described in Grainger et al. (2004).

20 3 Results

3.1 Optical properties of black carbon fractal aggregates

Figure 2 shows the extinction and scattering cross-sections, and asymmetry parameter for BCFAs as a function of D_f and n_s in the visible. Although not clear from the figure (due to the logarithmic scale), the extinction cross-section is broadly a function of 25 the particle volume suggesting that using the Rayleigh limit might be appropriate. The

Title Page	
Abstract	Introduction
Conclusions	References
Tables	Figures
	
	
Back	Close
Full Screen / Esc	
Printer-friendly Version	
Interactive Discussion	



scattering cross-section is more pronounced at higher D_f as the fractals become more densely packed and so a more coherent scattering entity. Similarly, g shows a greater amount of the light being scattered forwards as the fractals become both more densely packed, and larger.

- 5 Figure 3 shows the single scatter albedo ($\text{SSA} = \sigma_{\text{sca}}/\sigma_{\text{ext}}$) which agrees well with the literature review by Bond and Bergstrom (2006), who noted that when measured, the SSA of BCFAs are “surprisingly consistent” with a value of 0.2–0.3.

10 Since fractal aggregates are by nature randomly assembled, these are not the only possible representations of the light scattering properties that a BCFA with these properties could have. However, as shown in Fig. 4, relative difference from the mean values 15 of the three parameters are small, with variance in the total extinction generally less than 1 % away from the mean, and less than 5 % away for σ_{sca} and g at $\lambda = 550$ nm.

At $\lambda = 12$ μm , one might expect things to be more straightforward. The size parameter of the largest BCFAs studied are $x_V = 0.1$ and $x_G = 0.6$ (by equivalent volume and radius of gyration respectively) which would place the vast majority of studied equivalent spherical particles in the Rayleigh limit. In that case it would be expected that $g \approx 0$ and that there would be little dependency of the cross-sections with shape. Figure 5 shows BCFA light scattering at 12 μm , where the refractive index is $m_{\text{BC}} = 2.93 + 2.16i$.

20 For particles with large D_f values, the asymmetry is close to zero, but this is not the case for larger particles with smaller fractal dimensions.

The calculations over the entire wavelength range are shown in Fig. 6 at a fixed fractal dimension of $D_f = 1.8$. Extinction cross-sections decrease with decreasing size parameter (either because of increasing wavelength or decreasing numbers of spherules in the aggregate).

25 Single scatter albedo and asymmetry also decrease with decreasing size parameter and increasing k .

[Title Page](#)

[Abstract](#)

[Introduction](#)

[Conclusions](#)

[References](#)

[Tables](#)

[Figures](#)

◀

▶

◀

▶

[Back](#)

[Close](#)

[Full Screen / Esc](#)

[Printer-friendly Version](#)

[Interactive Discussion](#)



3.2 Finding appropriate spheres

For all of the BCFAs, it was attempted to find matching optical properties using spheres with $50 < r < 1500$ nm, $1 < n < 4$, and $0 < k < 4$. Attempting to fit closest values of $\ln \sigma_{\text{ext}}$, $\ln \sigma_{\text{sca}}$, and g using optimal estimation (Rodgers, 2000) is shown in Fig. 7 for $\lambda = 550$ nm.

Relative errors of $> 15\%$ for extinction, $> 20\%$ for scattering, and $> 40\%$ for asymmetry at this wavelength are unacceptable, and do not improve with increased wavelength. Similar attempts fitting the single scatter albedo instead of $\ln \sigma_{\text{sca}}$, and σ instead of $\ln \sigma$ values also were not successful. Least-square fits were also unsuccessful. As such, it is suggested that within the range $0.4 \leq \lambda \leq 15$ μm , there are no suitable sizes or refractive indices of spheres appropriate for the optical modelling of black carbon aggregates.

3.3 Parameterising fractal aggregate optical properties

Since the extinction cross-section scales with volume which is proportional to n_s , a polynomial in n_s was chosen and order 3 was found to adequately capture the full range of λ , D_f and n_s used here.

$$\sigma_{\text{ext}} = \sum_{m=0}^3 k_m n_s^m. \quad (2)$$

The scattering cross-section is not so simple to parameterise, and so the SSA is fitted instead and multiplied by σ_{ext} to obtain σ_{sca} . The SSA and g are both well captured by a logarithmic n_s and a linear offset. This was due to the tendency of these optical properties to initially increase with n_s before levelling off at large n_s :

$$\text{SSA} = w_0 + w_1 n_s + w_2 \ln n_s, \quad (3)$$

$$g = G_0 + G_1 n_s + G_2 \ln n_s. \quad (4)$$

[Title Page](#)

[Abstract](#)

[Introduction](#)

[Conclusions](#)

[References](#)

[Tables](#)

[Figures](#)

[|◀](#)

[▶|](#)

[◀](#)

[▶](#)

[Back](#)

[Close](#)

[Full Screen / Esc](#)

[Printer-friendly Version](#)

[Interactive Discussion](#)



[Title Page](#)[Abstract](#)[Introduction](#)[Conclusions](#)[References](#)[Tables](#)[Figures](#)[◀](#)[▶](#)[◀](#)[▶](#)[Back](#)[Close](#)[Full Screen / Esc](#)[Printer-friendly Version](#)[Interactive Discussion](#)

Table 1 shows the fit coefficients at 550 nm and $D_f = 1.8$. The root-mean-square (RMS) errors in σ_{ext} , SSA, and g compared to the calculated values are also given. Including the smallest particles is roughly responsible for a doubling in the error of the fits, as can be shown by not including the two smallest particle sizes in the calculation.

- 5 This is because the limit $\lim_{n_s \rightarrow 0}(\sigma_{\text{ext}}) = 0$ and $\lim_{n_s \rightarrow 0}(g) = 0$ leading to large inflation in the relative differences between points. Over the entire range of λ and D_f , errors in the visible are below 3 % as shown in Fig. 8. In the range $2 \leq \lambda \leq 9 \mu\text{m}$, RMS errors in SSA and g can be as large as 10 %. Errors in extinction are < 10 % in all cases.

3.4 Parameterising light scattering for a lognormal distribution of particles

- 10 From these fitted optical schemes, the optical properties of lognormal distributions of these particles can be obtained trivially. For the extinction, we first relate n_s to a size distribution by volume-equivalent radius, r , saying

$$r = a \sqrt[3]{n_s}, \quad (5)$$

and inserting into a lognormal distribution defined as:

$$15 n(r) = \frac{N}{\sigma r \sqrt{2\pi}} \exp \left[-\frac{1}{2} \left(\frac{\ln r - \ln r_0}{\sigma} \right)^2 \right], \quad (6)$$

where N is the total number of particles in the distribution, σ is the standard deviation of $\ln r$, and r_0 is the geometric mean of r . The extinction coefficient at some point along the path of a light beam, z , is defined as

$$\beta_{\text{ext}}(z) = \int_0^{\infty} \sigma_{\text{ext}}(r) n(r, z) dr. \quad (7)$$

Following from Eq. (2), σ_{ext} can be separated into four terms in powers of r^3 :

$$\sigma_{\text{ext}} = \sum_{i=0}^3 k_m \left(\frac{r}{a} \right)^{3m}. \quad (8)$$

Finally, noting that

$$\frac{1}{\sigma \sqrt{2\pi}} \int_0^\infty r^{m-1} \exp \left[-\frac{1}{2} \left(\frac{\ln \frac{r}{r_0}}{\sigma} \right)^2 \right] dr = r_0^m e^{\frac{m^2 \sigma^2}{2}}, \quad (9)$$

- ⁵ an expression for β_{ext} is given by

$$\beta_{\text{ext}} = N \sum_{m=0}^3 k_m \left(\frac{r_0}{a} \right)^{3m} e^{\frac{(3ma)^2}{2}}. \quad (10)$$

Scattering is obtained from the extinction and single scatter albedo as:

$$\begin{aligned} \beta_{\text{sca}}(z) &= \int_0^\infty \sigma_{\text{sca}}(r) n(r, z) dr = \int_0^\infty \sigma_{\text{ext}}(r) \text{SSA}(r) n(r, z) dr, \\ &= \int_0^\infty \sum_{m=0}^3 k_m \left(\frac{r}{a} \right)^{3m} \left[w_0 + w_1 \left(\frac{r}{a} \right)^3 + w_2 \ln \left(\frac{r}{a} \right)^3 \right] n(r, z) dr. \end{aligned} \quad (11)$$

10

Using

$$\frac{1}{\sigma \sqrt{2\pi}} \int_0^\infty r^{m-1} \ln r \exp \left[-\frac{1}{2} \left(\frac{\ln \frac{r}{r_0}}{\sigma} \right)^2 \right] dr = r_0^m e^{\frac{m^2 \sigma^2}{2}} (\ln r_0 + m\sigma^2), \quad (12)$$

Title Page	Abstract	Introduction
Conclusions	References	
Tables	Figures	
◀	▶	
◀	▶	
Back	Close	
Full Screen / Esc		
Printer-friendly Version		
Interactive Discussion		



Black carbon fractal aggregates

A. J. A. Smith and
R. G. Grainger[Title Page](#)[Abstract](#)[Introduction](#)[Conclusions](#)[References](#)[Tables](#)[Figures](#)[◀](#)[▶](#)[Back](#)[Close](#)[Full Screen / Esc](#)[Printer-friendly Version](#)[Interactive Discussion](#)

this can be reduced to

$$\beta_{\text{sca}} = N\beta_{\text{ext}}(w_0 - 3w_2 \ln a) + N \sum_{m=0}^3 k_m \left(\frac{r_0}{a}\right)^{3m} e^{\frac{(3m\sigma)^2}{2}} \times \left[w_1 \left(\frac{r_0}{a}\right)^3 e^{\frac{9\sigma^2(2m+1)}{2}} + 3w_2 (\ln r_0 + 3m\sigma) \right]. \quad (13)$$

- 5 Similar integration can be used to find the averaged asymmetry parameter for the size distribution, $\langle g \rangle$, using:

$$\langle g \rangle = \frac{\int_0^\infty \sigma_{\text{sca}}(r) g(r) n(r, z) dr}{\beta_{\text{sca}}}, \quad (14)$$

by noting that:

$$\frac{1}{\sigma\sqrt{2\pi}} \int_0^\infty r^{m-1} \ln^2 r \exp \left[-\frac{1}{2} \left(\frac{\ln \frac{r}{r_0}}{\sigma} \right)^2 \right] dr = r_0^m e^{\frac{m^2\sigma^2}{2}} [(\ln r_0 + m\sigma^2)^2 + \sigma^2]. \quad (15)$$

10 Using a reasonable atmospheric BC size distribution ($r_0 = 120 \text{ nm}$; $\sigma = \ln 1.32$), differences between the extinction calculated by summing the various individual fractal calculations, and the parameterisation were investigated. The method used is shown for the example of $\lambda = 2 \mu\text{m}$ and $D_f = 1.8$ in Fig. 9. The parameterisation is an integral over the whole of particle radius space, whereas the calculations of fractal optical properties were truncated at $n_s = 980$ ($r = 248 \text{ nm}$). As such to check the validity of the 15 integral parameterisation, the limit was set at $\int_0^{248 \text{ nm}} f(r) dr$. For all wavelengths and fractal dimensions, agreement between the two methods is within 3 % for g and σ_{sca} , and within 0.15 % for σ_{ext} . Errors are slightly smaller than for individual scattering particles, since the parameterisation of individual particles roughly underestimates values 20 as often as it overestimates.

The parameterisation is available as an Supplement to this work, and includes routines in the Interactive Data Language (IDL) to implement extinction, scattering, SSA,



and asymmetry parameter calculations for individual particles and log-normal distributions.

4 Conclusions

It has been shown that it is not possible to model the optical properties of black carbon fractal aggregates using spheres with refractive indices in the range $0 \leq m_{BC} \leq 3 + 3i$ at any wavelength between 400 nm and 15 μm . With this in mind, a prudent step for GCMs requiring constantly changing distributions of BC aerosol could be to include a parameterisation such as this one which is computationally trivial to implement and is valid within the range of black carbon particles seen in the atmosphere.

10 **Supplementary material related to this article is available online at
[http://www.atmos-chem-phys-discuss.net/14/3537/2014/
acpd-14-3537-2014-supplement.zip](http://www.atmos-chem-phys-discuss.net/14/3537/2014/acpd-14-3537-2014-supplement.zip).**

15 *Acknowledgement.* The authors acknowledge funding from the UK Natural Environment Research Council (NERC) National Centre for Earth Observation and the NERC project NE/F018142/1.

References

- Abel, S. J., Haywood, J. M., Highwood, E. J., Li, J., and Buseck, P. R.: Evolution of biomass burning aerosol properties from an agricultural fire in southern Africa, *Geophys. Res. Lett.*, 30, 1783, doi:10.1029/2003GL017342, 2003. 3540
- 20** Bahadur, R., Feng, Y., Russell, L. M., and Ramanathan, V.: Impact of California's air pollution laws on black carbon and their implications for direct radiative forcing, *Atmos. Environ.*, 45, 1162–1167, doi:10.1016/j.atmosenv.2010.10.054, 2011. 3538

[Title Page](#)

[Abstract](#)

[Introduction](#)

[Conclusions](#)

[References](#)

[Tables](#)

[Figures](#)

◀

▶

◀

▶

[Back](#)

[Close](#)

[Full Screen / Esc](#)

[Printer-friendly Version](#)

[Interactive Discussion](#)



Black carbon fractal aggregates

A. J. A. Smith and
R. G. Grainger

- Bohren, C. F. and Huffman, D. R.: Absorption and Scattering of Light by Small Particles, Wiley-VCH, doi:10.1002/9783527618156, 1983. 3541, 3542
- Bond, T. C.: Can warming particles enter global climate discussions?, *Environ. Res. Lett.*, 2, 045030, doi:10.1088/1748-9326/2/4/045030, 2007. 3538
- 5 Bond, T. C. and Bergstrom, R. W.: Light absorption by carbonaceous particles: an investigative review, *Aerosol Sci. Tech.*, 40, 27–67, doi:10.1080/02786820500421521, 2006. 3542, 3543
- Bond, T. C., Streets, D. G., Yarber, K. F., Nelson, S. M., Woo, J.-H., and Klimont, Z.: A technology-based global inventory of black and organic carbon emissions from combustion, *J. Geophys. Res.*, 109, D14203, doi:10.1029/2003JD003697, 2004. 3538
- 10 Bond, T. C., Habib, G., and Bergstrom, R. W.: Limitations in the enhancement of visible light absorption due to mixing state, *J. Geophys. Res.*, 111, D20211, doi:10.1029/2006JD007315, 2006. 3540
- Bond, T. C., Doherty, S. J., Fahey, D. W., Forster, P. M., Berntsen, T., DeAngelo, B. J., Flanner, M. G., Ghan, S., Kärcher, B., Koch, D., Kinne, S., Kondo, Y., Quinn, P. K., Sarofim, M. C., Schultz, M. G., Schulz, M., Venkataraman, C., Zhang, H., Zhang, S., Bellouin, N., Guttienda, S. K., Hopke, P. K., Jacobson, M. Z., Kaiser, J. W., Klimont, Z., Lohmann, U., Schwarz, J. P., Shindell, D., Storelvmo, T., Warren, S. G., and Zender, C. S.: Bounding the role of black carbon in the climate system: a scientific assessment, *J. Geophys. Res.*, 118, 5380–5552, doi:10.1002/jgrd.50171, 2013. 3538, 3539
- 15 20 Buseck, P. R., Huang, B., and Keller, L. P.: Electron microscope investigation of the structures of annealed carbons, *Energ. Fuel.*, 1, 105–110, doi:10.1021/ef00001a020, 1987. 3540
- Calcote, H. F.: Mechanisms of soot nucleation in flames – a critical review, *Combust. Flame*, 42, 215–242, doi:10.1016/0010-2180(81)90159-0, 1981. 3539, 3540
- 25 Chang, H. and Charalampopoulos, T. T.: Determination of the wavelength dependence of refractive indices of flame soot, *P. Roy. Soc. Lond. A Mat.*, 430, 577–591, doi:10.1098/rspa.1990.0107, 1990. 3542
- Dockery, D. W., Pope, C. A., Xu, X., Spengler, J. D., Ware, J. H., Fay, M. E., Ferris, B. G., and Speizer, F. E.: An association between air pollution and mortality in six U. S. cities, *New Engl. J. Med.*, 329, 1753–1759, doi:10.1056/NEJM199312093292401, 1993. 3539
- 30 Doherty, S. J., Warren, S. G., Grenfell, T. C., Clarke, A. D., and Brandt, R. E.: Light-absorbing impurities in Arctic snow, *Atmos. Chem. Phys.*, 10, 11647–11680, doi:10.5194/acp-10-11647-2010, 2010. 3538

[Title Page](#)[Abstract](#)[Introduction](#)[Conclusions](#)[References](#)[Tables](#)[Figures](#)[◀](#)[▶](#)[Back](#)[Close](#)[Full Screen / Esc](#)[Printer-friendly Version](#)[Interactive Discussion](#)

Black carbon fractal aggregates

A. J. A. Smith and
R. G. Grainger

- Flanner, M. G., Zender, C. S., Hess, P. G., Mahowald, N. M., Painter, T. H., Ramanathan, V., and Rasch, P. J.: Springtime warming and reduced snow cover from carbonaceous particles, *Atmos. Chem. Phys.*, 9, 2481–2497, doi:10.5194/acp-9-2481-2009, 2009. 3538
- Fuller, K. A., Malm, W. C., and Kreidenweis, S. M.: Effects of mixing on extinction by carbonaceous particles, *J. Geophys. Res.*, 104, 15941–15954, doi:10.1029/1998JD100069, 1999. 3540
- Grainger, R. G., Lucas, J., Thomas, G. E., and Ewen, G. B.: Calculation of Mie derivatives, *Appl. Optics*, 43, 5386–5393, doi:10.1364/AO.43.005386, 2004. 3541, 3542
- Helble, J., Neville, M., and Sarofim, A. F.: Aggregate formation from vaporized ash during pulverized coal combustion, *Symposium (International) on Combustion*, 21, 411–417, doi:10.1016/S0082-0784(88)80268-6, 1988. 3539, 3540
- Homann, K. H.: Carbon formation in premixed flames, *Combust. Flame*, 11, 265–287, doi:10.1016/0010-2180(67)90017-X, 1967. 3540
- Ito, A. and Penner, J. E.: Historical emissions of carbonaceous aerosols from biomass and fossil fuel burning for the period 1870–2000, *Global Biogeochem. Cy.*, 19, GB2028, doi:10.1029/2004GB002374, 2005. 3538
- Jacobson, M. Z.: Strong radiative heating due to the mixing state of black carbon in atmospheric aerosols, *Nature*, 409, 695–697, doi:10.1038/35055518, 2001. 3538, 3540
- Jacobson, M. Z.: Control of fossil-fuel particulate black carbon and organic matter, possibly the most effective method of slowing global warming, *J. Geophys. Res.*, 107, 4410, doi:10.1029/2001JD001376, 2002. 3538
- Jacobson, M. Z.: Reply to comment by J. E. Penner on “Control of fossil-fuel particulate black carbon and organic matter, possibly the most effective method of slowing global warming”, *J. Geophys. Res.*, 108, 4772, doi:10.1029/2003JD003403, 2003. 3538
- Jansen, K. L., Larson, T. V., Koenig, J. Q., Mar, T. F., Fields, C., Stewart, J., and Lippmann, M.: Associations between health effects and particulate matter and black carbon in subjects with respiratory disease, *Environ. Health Persp.*, 113, 1741–1746, doi:10.1289/ehp.8153, 2005. 3539
- Larson, S. M., Cass, G. R., and Gray, H. A.: Atmospheric carbon particles and the Los Angeles visibility problem, *Aerosol Sci. Tech.*, 10, 118–130, doi:10.1080/02786828908959227, 1989. 3539
- Li, H., Liu, C., Bi, L., Yang, P., and Kattawar, G. W.: Numerical accuracy of “equivalent” spherical approximations for computing ensemble-averaged scattering properties of fractal soot ag-

[Title Page](#)[Abstract](#)[Introduction](#)[Conclusions](#)[References](#)[Tables](#)[Figures](#)[◀](#)[▶](#)[◀](#)[▶](#)[Back](#)[Close](#)[Full Screen / Esc](#)[Printer-friendly Version](#)[Interactive Discussion](#)

Black carbon fractal aggregates

A. J. A. Smith and
R. G. Grainger[Title Page](#)[Abstract](#)[Introduction](#)[Conclusions](#)[References](#)[Tables](#)[Figures](#)[◀](#)[▶](#)[◀](#)[▶](#)[Back](#)[Close](#)[Full Screen / Esc](#)[Printer-friendly Version](#)[Interactive Discussion](#)

gregates, *J. Quant. Spectrosc. Ra.*, **111**, 2127–2132, doi:10.1016/j.jqsrt.2010.05.009, 2010.
3542

Li, J., Pósfai, M., Hobbs, P. V., and Buseck, P. R.: Individual aerosol particles from biomass burning in southern Africa: 2. Compositions and aging of inorganic particles, *J. Geophys. Res.*, **108**, 8484, doi:10.1029/2002JD002310, 2003. 3540

Liu, L. and Mishchenko, M. I.: Effects of aggregation on scattering and radiative properties of soot aerosols, *J. Geophys. Res.*, **110**, D11211, doi:10.1029/2004JD005649, 2005. 3542

Mackowski, D. W.: MSTM – a multiple sphere T-matrix FORTRAN code for use on parallel computer clusters, Department of Mechanical Engineering, Auburn University, Auburn, AL 36849, USA, available at: <http://eng.auburn.edu/users/dmckwski/scatcodes> (last access: June 2013), 2012. 3541

Mackowski, D. W. and Mishchenko, M. I.: Calculation of the T-matrix and the scattering matrix for ensembles of spheres, *J. Opt. Soc. Am. A.*, **13**, 2266–2278, doi:10.1364/JOSAA.13.002266, 1996. 3541

Martins, J. V., Artaxo, P., Lioussse, C., Reid, J. S., Hobbs, P. V., and Kaufman, Y. J.: Effects of black carbon content, particle size, and mixing on light absorption by aerosols from biomass burning in Brazil, *J. Geophys. Res.*, **103**, 32041–32050, doi:10.1029/98JD02593, 1998a. 3540

Martins, J. V., Hobbs, P. V., Weiss, R. E., and Artaxo, P.: Sphericity and morphology of smoke particles from biomass burning in Brazil, *J. Geophys. Res.*, **103**, 32051–32057, doi:10.1029/98JD01153, 1998b. 3540

Mie, G.: Beiträge zur Optik trüber Medien, speziell kolloidaler Metallösungen, *Ann. Phys.*, **25**, 377–445, a translation can be found at <http://diogenes.iwt.uni-bremen.de/vt/laser/papers/RAE-LT1873-1976-Mie-1908-translation.pdf> (last access: 15 March 2011), 1908. 3541

Popovicheva, O., Persiantseva, N. M., Shonija, N. K., DeMott, P., Koehler, K., Petters, M., Kreidenweis, S., Tishkova, V., Demirdjian, B., and Suzanne, J.: Water interaction with hydrophobic and hydrophilic soot particles, *Phys. Chem. Chem. Phys.*, **10**, 2332–2344, doi:10.1039/b718944n, 2008. 3540

Pósfai, M., Anderson, J. R., Buseck, P. R., and Sievering, H.: Soot and sulfate aerosol particles in the remote marine troposphere, *J. Geophys. Res.*, **104**, 21685–21693, doi:10.1029/1999JD900208, 1999. 3540

Black carbon fractal aggregates**A. J. A. Smith and
R. G. Grainger**

- Reid, J. S., Koppmann, R., Eck, T. F., and Eleuterio, D. P.: A review of biomass burning emissions part II: intensive physical properties of biomass burning particles, *Atmos. Chem. Phys.*, 5, 799–825, doi:10.5194/acp-5-799-2005, 2005. 3539, 3540
- Rodgers, C. D.: *Inverse Methods for Atmospheric Sounding: Theory and Practice*, vol. 2 of *Atmospheric, Oceanic and Planetary Physics*, World Scientific Publishing Co., 2000. 3542, 3544
- Sorensen, C. M.: Light scattering by fractal aggregates: a review, *Aerosol Sci. Tech.*, 35, 648–687, doi:10.1080/02786820117868, 2001. 3540, 3541
- Stier, P., Seinfeld, J. H., Kinne, S., and Boucher, O.: Aerosol absorption and radiative forcing, *Atmos. Chem. Phys.*, 7, 5237–5261, doi:10.5194/acp-7-5237-2007, 2007. 3542
- Streets, D. G., Bond, T. C., Carmichael, G. R., Fernandes, S. D., Fu, Q., He, D., Klimont, Z., Nelson, S. M., Tsai, N. Y., Wang, M. Q., Woo, J.-H., and Yarber, K. F.: An inventory of gaseous and primary aerosol emissions in Asia in the year 2000, *J. Geophys. Res.*, 108, 8809, doi:10.1029/2002JD003093, 2003. 3538
- Thouy, R. and Jullien, R.: A cluster–cluster aggregation model with tunable fractal dimension, *J. Phys. A-Math. Gen.*, 27, 2953, doi:10.1088/0305-4470/27/9/012, 1994. 3542
- Turns, S. R.: *An Introduction to Combustion – Concepts and Applications*, 2nd edn., McGraw-Hill, 2000. 3539, 3540
- Zhang, R., Khalizov, A. F., Pagels, J., Zhang, D., Xue, H., and McMurry, P. H.: Variability in morphology, hygroscopicity, and optical properties of soot aerosols during atmospheric processing, *P. Natl Acad. Sci. USA*, 105, 10291–10296, doi:10.1073/pnas.0804860105, 2008. 3540
- Zhao, Y. and Ma, L.: Applicable range of the Rayleigh–Debye–Gans theory for calculating the scattering matrix of soot aggregates, *Appl. Optics*, 48, 591–597, doi:10.1364/AO.48.000591, 2009. 3542

Title Page	
Abstract	Introduction
Conclusions	References
Tables	Figures
◀	▶
◀	▶
Back	Close
Full Screen / Esc	
Printer-friendly Version	
Interactive Discussion	



Black carbon fractal aggregates

A. J. A. Smith and
R. G. Grainger

Table 1. Fit coefficients for estimation of BCFA optical properties at $\lambda = 550$ nm and $D_f = 1.8$. Relative RMS errors for all fitted points, equally weighted are also given. The marked, lower values, “Rel.” ignore the first two data points where $n_s \leq 40$, showing that this is where the majority of the relative error is contained.

Coeff.	σ_{ext}	SSA	g
0	-2.026×10^3	8.902×10^{-2}	2.669×10^{-1}
1	9.581×10^2	0.000×10^0	0.000×10^0
2	1.120×10^{-3}	2.876×10^{-2}	6.981×10^{-2}
3	4.110×10^{-6}	—	—
RMS error			
Rel.	0.50 %	2.53 %	5.02 %
Rel.*	0.25 %	1.64 %	2.13 %

[Title Page](#)[Abstract](#)[Introduction](#)[Conclusions](#)[References](#)[Tables](#)[Figures](#)[|◀](#)[▶|](#)[Back](#)[Close](#)[Full Screen / Esc](#)[Printer-friendly Version](#)[Interactive Discussion](#)

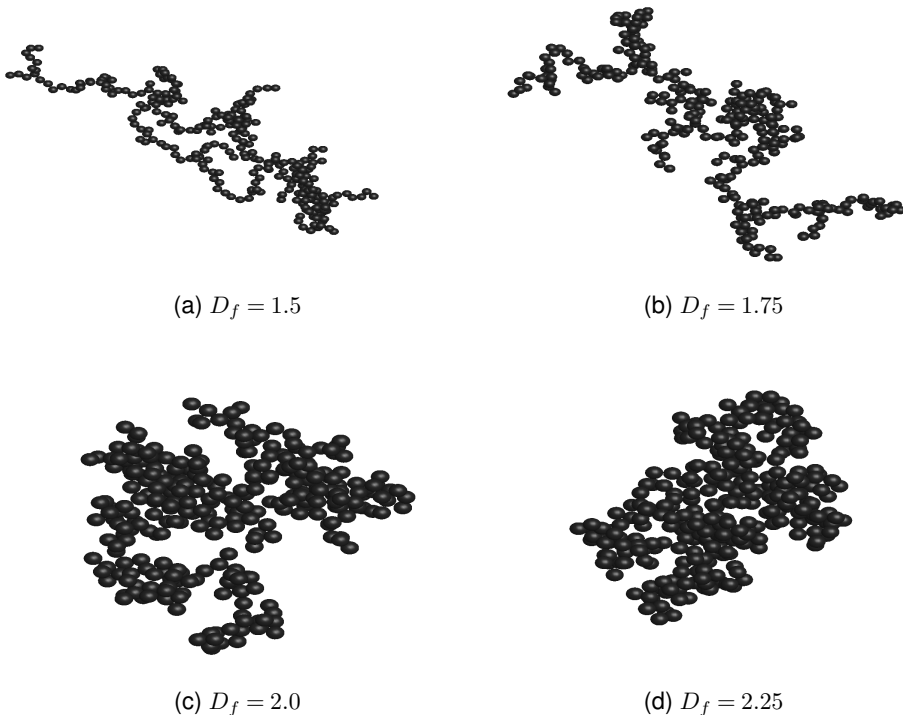
Black carbon fractal aggregatesA. J. A. Smith and
R. G. Grainger

Fig. 1. Modelled fractal aggregates with $N = 300$, $k_f = 1.25$ and varying values of D_f . As the fractal dimension increases, we move from linear to bunched clusters. These aggregates were generated using a cluster-cluster algorithm.

[Title Page](#)[Abstract](#)[Introduction](#)[Conclusions](#)[References](#)[Tables](#)[Figures](#)[|◀](#)[▶|](#)[◀](#)[▶](#)[Back](#)[Close](#)[Full Screen / Esc](#)[Printer-friendly Version](#)[Interactive Discussion](#)

Black carbon fractal aggregates

A. J. A. Smith and
R. G. Grainger

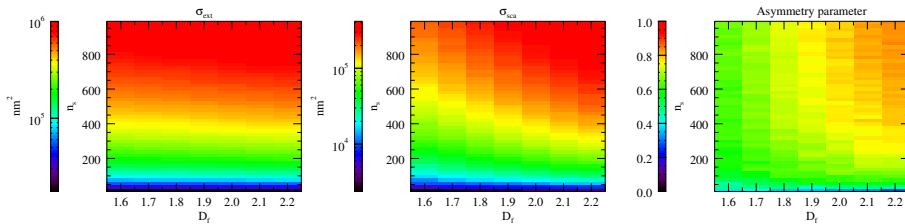


Fig. 2. Extinction cross-section, scattering cross-section, and asymmetry parameter calculated using the MSTM code at $\lambda = 550$ nm for a range of fractal dimensions and numbers of spherules.

- [Title Page](#)
- [Abstract](#) [Introduction](#)
- [Conclusions](#) [References](#)
- [Tables](#) [Figures](#)
- [◀](#) [▶](#)
- [◀](#) [▶](#)
- [Back](#) [Close](#)
- [Full Screen / Esc](#)
- [Printer-friendly Version](#)
- [Interactive Discussion](#)

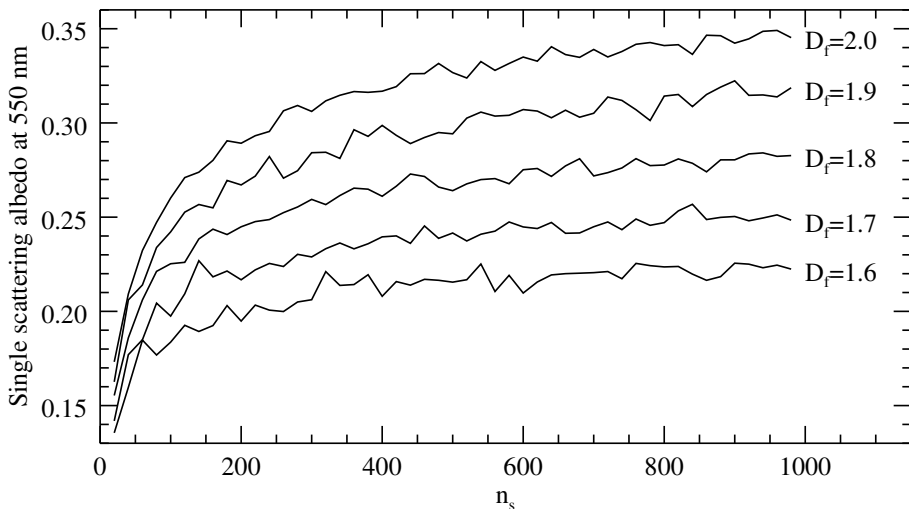


Fig. 3. The SSA of BCFAs at $\lambda = 550$ nm as a function of n_s and D_f . The most likely values of D_f would be from 1.7–1.8, where the SSA values are between 0.2–0.3.

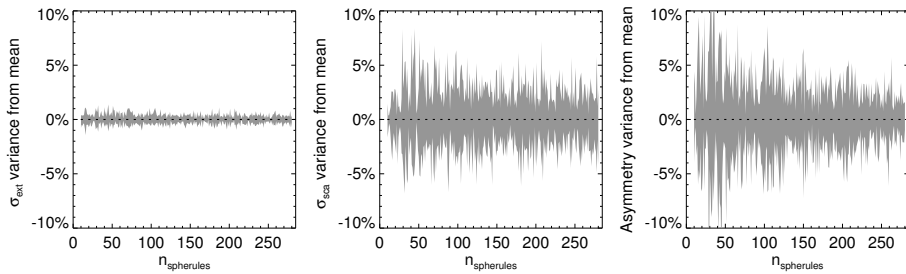
Black carbon fractal aggregatesA. J. A. Smith and
R. G. Grainger

Fig. 4. Showing the envelope of relative spread from the mean of the three output parameters, σ_{ext} , σ_{sca} and g at $\lambda = 550 \text{ nm}$, for BC with $D_f = 1.75$, given four fractal geometries at each size. The high relative differences g with low n_s can be accounted for by the lower values of g in this regime.

- [Title Page](#)
- [Abstract](#) [Introduction](#)
- [Conclusions](#) [References](#)
- [Tables](#) [Figures](#)
- [◀](#) [▶](#)
- [◀](#) [▶](#)
- [Back](#) [Close](#)
- [Full Screen / Esc](#)
- [Printer-friendly Version](#)
- [Interactive Discussion](#)



Black carbon fractal aggregates

A. J. A. Smith and
R. G. Grainger

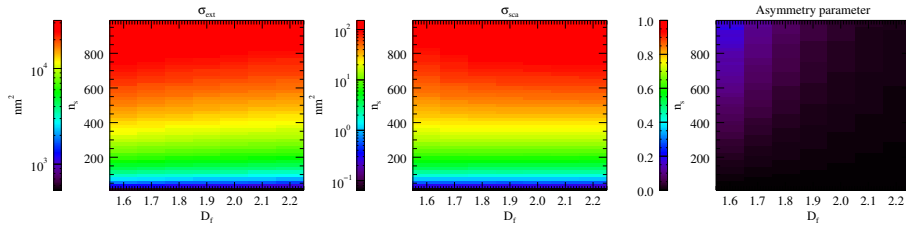


Fig. 5. Extinction cross-section, scattering cross-section, and asymmetry parameter calculated using the MSTM code at $\lambda = 12 \mu\text{m}$ for a range of fractal dimensions and numbers of spherules.

[Title Page](#)
[Abstract](#) [Introduction](#)
[Conclusions](#) [References](#)
[Tables](#) [Figures](#)

[◀](#) [▶](#)
[◀](#) [▶](#)
[Back](#) [Close](#)
[Full Screen / Esc](#)

[Printer-friendly Version](#)
[Interactive Discussion](#)



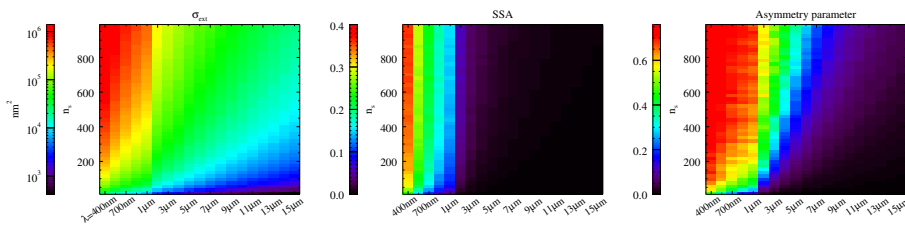
Black carbon fractal aggregatesA. J. A. Smith and
R. G. Grainger

Fig. 6. Extinction cross-section, single scatter albedo, and asymmetry parameter calculated using the MSTM code at $D_f = 1.8$. Note the discontinuity in wavelength step size at $\lambda = 1 \mu\text{m}$. Unlabeled wavelengths are half-way between the two values on either side.

[Title Page](#)[Abstract](#)[Introduction](#)[Conclusions](#)[References](#)[Tables](#)[Figures](#)[|◀](#)[▶|](#)[Back](#)[Close](#)[Full Screen / Esc](#)[Printer-friendly Version](#)[Interactive Discussion](#)

Black carbon fractal aggregates

A. J. A. Smith and
R. G. Grainger

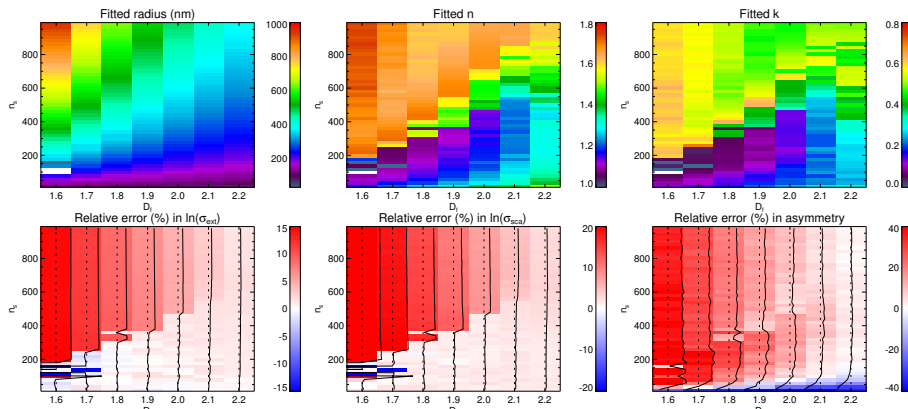


Fig. 7. The optimum fitted sphere parameters (r , n , and k) and their resultant relative errors in $\ln\sigma_{ext}$, $\ln\sigma_{sca}$ and g .

Black carbon fractal aggregates

A. J. A. Smith and
R. G. Grainger

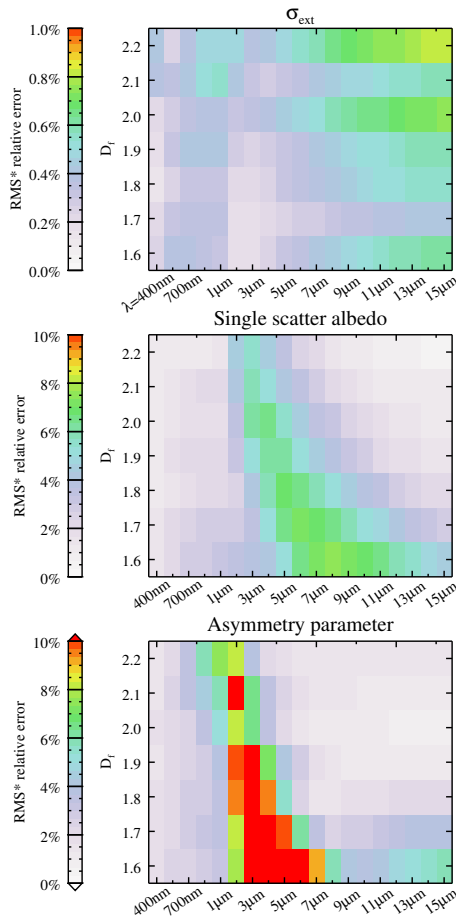


Fig. 8. The RMS relative errors between the calculated and parameterised values of σ_{ext} , SSA, and g . RMS calculations exclude the lowest two values of n_s as discussed in the text.

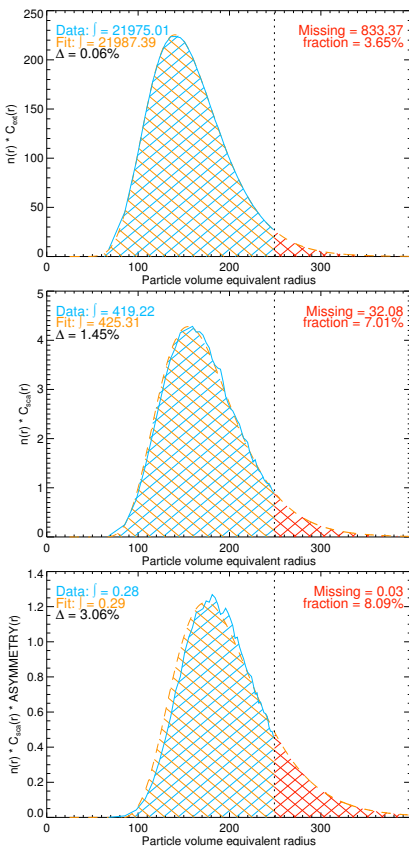


Fig. 9. Comparing the integrals of extinction, scattering, and asymmetry from a sum of fractal optical properties, and the parameterisations described in the text. Differences between the parameterised fit and the data are compared only for the area bounded by the maximum value of $n_s = 980$. These calculations are for $D_f = 1.8$ and $\lambda = 2 \mu\text{m}$.

3562

 CC BY